Imaging of Longitudinal Electron Focusing by Light-Induced Carrier Excitation

M. Primke, J. Heil, A. Böhm, A. Gröger, and P. Wyder

Hochfeld-Magnetlabor, Max-Planck-Institut für Festkörperforschung and Centre National de la Recherche Scientifique, B.P. 166, 25 Avenue des Martyrs, F-38042 Grenoble Cedex 9, France

(Received 3 July 1996; revised manuscript received 29 January 1997)

We report on the two-dimensional observation of electron focusing under the influence of a longitudinal magnetic field B_l using a real space imaging technique. As a function of B_l the focusing patterns are modified and shrink together in good qualitative agreement with calculated focusing patterns of ballistic electrons. At low fields we observed Sondheimer oscillations periodic in B_l. At high fields light-induced magneto-oscillations due to Landau quantization occur. [S0031-9007(97)04760-1]

PACS numbers: 72.15.Eb, 03.65.Sq, 72.15.Jf, 75.80.+q

The electronic mean free path l^* in metals at room temperature is of the order of nm and therefore in the range of interatomic distances [1]. In very pure single crystals at low temperatures T, l^* can reach values of several 100 μm. Under these conditions it is possible to perform experiments in the so-called ballistic regime, where l^* is of the order of typical sample dimensions.

Sharvin [2], for example, fixed two point contacts (PC) on opposite surfaces of a Sn sample. One PC (emitter) was used to inject carriers into the crystal and the other PC (collector) detected the collector voltage V_c. For certain values of a longitudinal magnetic field B_l (along the line connecting emitter and collector, Sharvin geometry) he observed peaks in V_c, a phenomenon which he called longitudinal electron focusing.

We recently presented a new experimental technique which allows one to image the far field radiation pattern of a carrier point source [3–6]. The real space imaging capability makes this technique the ideal tool for studies of the spatial distribution of the trajectories of carriers under the influence of a magnetic field, for example in the Sharvin geometry. These Sharvin-type experiments using this new technique are presented here for the first time. The advantage over the classical Sharvin experiment is the possibility to observe the changes of the carrier flux pattern induced by the application of $\mathbf{B}_l$ not only at a given location, but on the whole sample surface.

The experimental setup presented in Fig. 1(a) is similar to the one described in [3,6]. The beam of a 30 mW Ar laser is coupled into an optical fiber which illuminates a small spot of the surface of a Bi single crystal slab of thickness $d \approx l^*$. As previous work indicated, "hot electrons" are thermally excited, spread out from the illuminated spot, and propagate nearly ballistically (without scattering) towards the opposite surface of the crystal. Within the ballistic regime the carrier propagation in metals is in general highly anisotropic and is mainly determined by the shape of the Fermi surface [5]. At the opposite surface of the sample the incoming carrier flux is detected by a collector point contact. The focusing pattern is obtained by recording the voltage V_c at the collector as a function of the position of the hot electron excitation (see [3] for details).

Typical experimental results, recorded on the trigonal surface of a Bi single crystal slab of the thickness $d \approx 230$ μm at $T = 1.5$ K, are shown in Fig. 2. V_c is presented in gray scale as a function of the fiber position for different values of B_l such that the electron signal appears bright.

The observation of the focusing pattern for $B = 0$ T presented in Fig. 2(a) and the underlying mechanism have

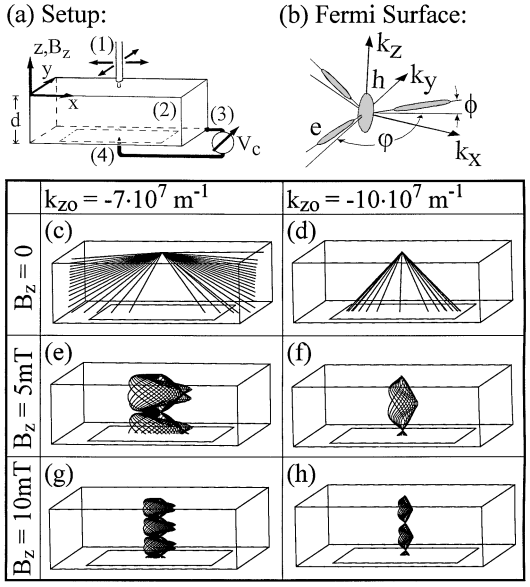

FIG. 1. (a) Scheme of the experimental setup. A small area $\approx(20\ \mu\text{m})^2$ on the sample (2) is illuminated with an optical fiber (1). The voltage V_c at the collector point contact (4) is measured with respect to a reference contact (3). (b) The Fermi surface of Bi consists of one hole ellipsoid and three extremely stretched electron ellipsoids with $\phi = 120°$ and $\theta \approx 6°$ [7]. (c)–(h) Calculated electron trajectories of ballistic electrons which emerge from a point source on the upper surface of the sample (for clarity only one of the Fermi ellipsoids with a fixed value of k_z is used). The size of the image frame that corresponds to the theoretical focusing patterns (Fig. 4) is indicated on the lower sample surface.

 0031-9007/97/79(24)/4882(4)$10.00

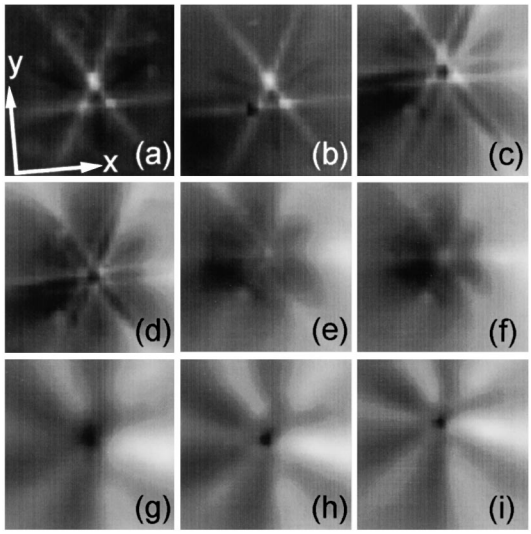

FIG. 2. Experimental focusing patterns for different values of the longitudinal magnetic field: The voltage V_c at the collector is shown in gray scale as a function of the fiber position. The image frame is approximately $(450\ \mu\text{m})^2$. (a) $B = 0$ T; (b) $B = 1.1$ mT; (c) $B = 1.7$ mT; (d) $B = 2.3$ mT; (e) $B = 2.8$ mT; (f) $B = 4.5$ mT; (g) $B = 25$ mT; (h) $B = 50$ mT; (i) $B = 75$ mT.

already been discussed in [3]: The Fermi surface of Bi consists of three extremely stretched electron ellipsoids as shown in Fig. 1(b). Without magnetic field the carrier propagation is highly enhanced in planes perpendicular to the long axes of the Fermi ellipsoids. These planes intersect with the opposite sample surface in three straight lines which are observed in the center of the focusing pattern. In addition to this electronic signal, three dark lines emerge from the center in the directions between the bright lines. This dark structure is related to phonons [3].

In the case of rather small transverse magnetic fields (parallel to the sample surface) of the order of 1 mT the contributions of ballistic electrons are already completely suppressed. For longitudinal magnetic fields, however, the electronic contributions are expected to remain visible even at high magnetic fields. This expectation is confirmed by the experimental results presented in Fig. 2. As a general trend the range of V_c increases with B from $27\ \text{nV} \le V_c \le 90\ \text{nV}$ for $B = 0$ T to $-920\ \text{nV} \le V_c \le 540\ \text{nV}$ for $B_l = 75$ mT. All experimental focusing patterns are scaled to the minimum (black) and maximum (white) values of V_c.

Because of the symmetry of the high field focusing patterns we expected to obtain an alignment of the collector and the source with the magnetic field by placing the fiber in the center of the patterns. Here an experiment similar to that of Sharvin [2] was performed by measuring V_c as a function of B_l. However, in our experiment light induced carrier excitation was used instead of carrier injection. The result at low magnetic fields is presented in Fig. 3(a). The field dependence of V_c is approximately symmetric with a maximum at $B = 0$ T. Peaks roughly equally spaced in B_l are observed. For higher fields V_c takes large negative values.

Figure 4 shows the theoretical focusing patterns calculated by a Monte Carlo simulation using the semiclassical model of electron dynamics, as proposed in [4]. For the calculations the so-called ellipsoidal-parabolic band structure approximation

$$\epsilon(\mathbf{k}) = \frac{\hbar^2}{2m}\left(A_x k_x^2 + A_y k_y^2 + A_z k_z^2 + 2A_{yz} k_y k_z\right) \quad (1)$$

is used with $A_x = 202$, $A_y = 1.67$, $A_z = 70$, $A_{yz} = 7.0$ [8]. The Fermi energy is $\varepsilon_F = 17.7$ meV and m is the free electron mass. The advantage of this simplified band structure approximation is that the semiclassical equations of motion [1] for a uniform magnetic field B_z can be

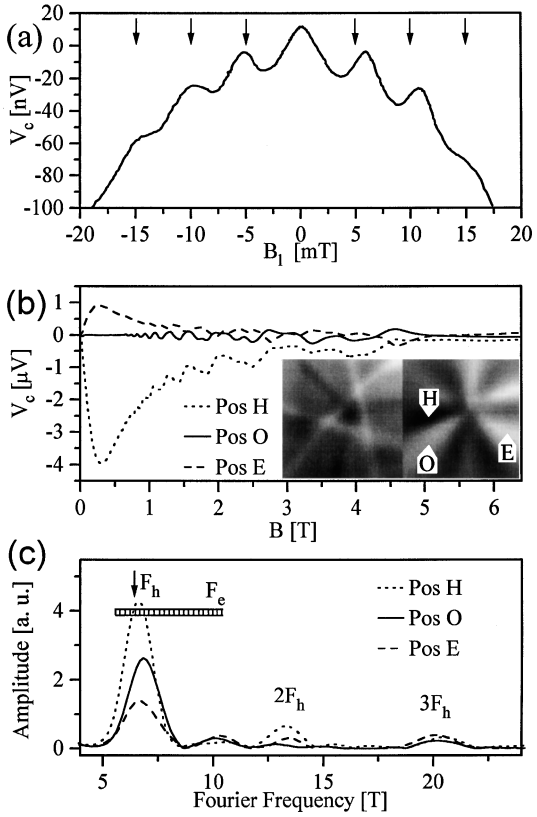

FIG. 3. (a) Light-induced longitudinal electron focusing in Bi. The voltage V_c is measured as a function of a longitudinal magnetic field in the Sharvin geometry. The fiber is positioned in the center of symmetry of Fig. 2(i). The arrows indicate the theoretically expected fields of the d.c. size effect oscillations. (b) V_c as a function of a magnetic field B approximately parallel to the trigonal axis of Bi at three different positions of excitation. The gray scale images show the corresponding electron focusing patterns at $B = 0$ T ($-8.1\ \text{nV} \le V_c \le -0.3$ nV) and $B = 30$ mT ($-840\ \text{nV} \le V_c \le 285$ nV) with an image frame of $(450\ \mu\text{m})^2$. (c) Fourier spectra of the $V_c(1/B_z)$ curves of (b). The de Haas–van Alphen frequencies for holes F_h and electrons F_e are indicated with the possible range for F_e for a tilt of the field with respect to the trigonal axis of the crystal up to 5° as a shaded horizontal bar.

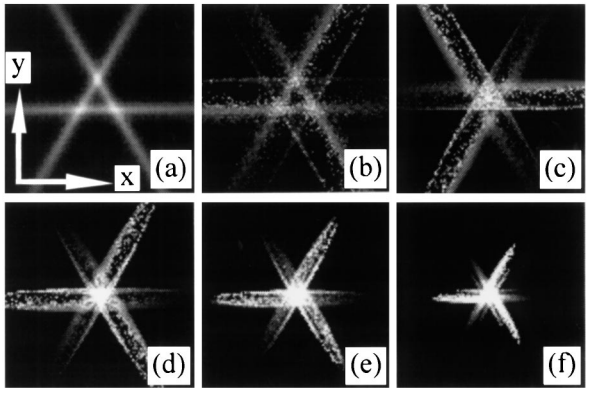

FIG. 4. Theoretical focusing pattern for different values of the longitudinal magnetic field. The image frame is $(400\ \mu\text{m})^2$ and the sample thickness is $d = 200\ \mu$m. The fields correspond to those shown in Figs. 2(a)–2(f). (a) $B = 0$ T; (b) $B = 1.1$ mT; (c) $B = 1.7$ mT; (d) $B = 2.3$ mT; (e) $B = 2.8$ mT; (f) $B = 4.5$ mT. The patterns are calculated with 10^7 events for $B = 0$ T and with 10^5 events for $B \neq 0$ T using the model described in [4].

solved analytically and not only numerically as in [4,5]. Some calculated electron trajectories for different values of k_z and B_z are presented in Figs. 1(c)–1(h).

Longitudinal focusing occurs when the electrons reach the opposite surface after an integer number n of revolutions. The condition can be obtained by solving the semiclassical equations of electron dynamics, or by using Sharvin's focusing condition [2] that the propagation g along a magnetic field in z direction during one revolution is

$$g = \frac{\hbar}{eB_z}\left(\frac{\partial S_{k_z}}{\partial k_z}\right)_{\epsilon=\text{const}}, \tag{2}$$

where S_{k_z} is the area of intersection of the Fermi surface with a plane $k_z = \text{const}$.

For the band structure in (1) both approaches lead to the longitudinal focusing condition:

$$B_{\text{foc}} = n\,\frac{k_{z0}}{d}\,\frac{2\pi\hbar}{e}\left(A_z - \frac{A_{yz}^2}{A_y}\right)(A_x A_y)^{-1/2}. \tag{3}$$

This is equivalent to the condition for oscillations of the Sondheimer effect (d.c. size effect) [9]. Here the contributions for different values of k_z are reported to interfere destructively, so that only feeble oscillations survive, with B_{foc}^* that corresponds to a limiting wave vector k_z^* of the Fermi surface [9]. For the band structure in (1) we obtain $k_z^* = 1.08 \times 10^8\ \text{m}^{-1}$ which gives $B_{\text{foc}}^* = n \times 4.8$ mT.

In the following we discuss the modifications of the focusing patterns under the influence of a longitudinal magnetic field. For increasing B_l, a second set of bright lines parallel to the first one appears [see Figs. 2(c) and 2(d)]. A similar behavior is observed in the theoretical focusing patterns in Figs. 4(c) and 4(d). For higher fields, the theoretical focusing patterns shrink together due to the scaling of the real space trajectories with $1/B_l$ perpendicular to $\mathbf{B}_l$. The corresponding bright spot can be observed in the center of symmetry of the experimental focusing pattern in Fig. 4(f).

The dark shadow region of Fig. 2(e), which shrinks together to a point for increasing B_l as in Fig. 2(i), may be interpreted as a diffuse contribution of the holes which surmounts the electronic signal for $B_l > 25$ mT. For $B_l < 25$ mT the hole contribution is expected to be small because of two reasons: First, the hole ellipsoid in the Fermi surface [see Fig. 1(b)] is not stretched in the same way as the electron ellipsoids, which results in a smooth, but not focused contribution over the whole pattern. Second, the mean free path of holes in Bi is much smaller than that of the electrons [10], which leads to a faster decay of the hole contribution with distance. With increasing field this behavior changes: If B_l is sufficiently high, even for a large number of scattering processes in the bulk, the hole trajectories are restricted to a narrow cone around the field axes, having a common origin in the illuminated spot. The opening angle of this cone increases with the number of scattering processes and decreases with increasing B_l. The dominance of the hole signal over the electronic signal at high B_l is presumably due to a phonon drag effect. Already the pattern at $B = 0$ T indicates that the coupling of the phonons to the holes is stronger than to the electrons, because the phonon signal (dark structure) has the opposite sign with respect to the electron signal (bright).

The origin of the fanlike structure observed around the dark spot at high fields [Fig. 2(g)–2(i)] is not yet understood. It is remarkable that the pattern evolves from threefold symmetry for $B = 0$ T to sixfold symmetry for high fields. The different modes of calculated phonon focusing patterns do not correspond to this fanlike structure. Because of its extension, it cannot be related to purely ballistic carrier propagation, but may be some diffusive process, probably related to the anisotropy of the magnetoresistance.

From the observations mentioned above, the $V_c(B_l)$ characteristic in Fig. 3(a) can be interpreted as being composed of at least two contributions. The first one describes the general behavior due to a concentration of diffusive hole flux onto the collector of finite area. Since the trajectories scale in the xy plane with $1/B_l$, one should expect V_c to be quadratic in B_l, which is in good qualitative agreement with the behavior of the signal in Fig. 3(a). In addition, the signal shows oscillations roughly periodic in B_l and the period corresponds approximately to the theoretical value $B_z^* = n \times 4.8$ mT of Sondheimer oscillations.

The $V_c(B)$ characteristics at high magnetic fields are shown in Fig. 3(b) for different positions of the illuminated spot with respect to the collector point contact. The positions are indicated in the inset of the focusing pattern for $B = 30$ mT, recorded on a Bi single crystal slab of the thickness $d \approx 400\ \mu$m. These patterns are similar to those of Fig. 2 but they do not show the dark

spot expected at higher fields, probably due to a small tilt between the crystal and the field axis. Pos E, Pos H and Pos O are situated near the maximum, minimum, or correspondingly zero value of V_c in the focusing pattern for $B = 30$ mT. Within our convention for V_c used in the gray scale patterns, the electron signal appears bright (Pos E) and the hole signal is shown dark (Pos H).

All measured $V_c(B)$ curves (only three are presented here) show magneto-oscillations periodic in $1/B$, on a background which is increasing to a maximum value at $B \approx 0.3$ T and with a strong decay towards high fields.

The Fourier amplitude spectra of the $V_c(1/B)$ curves depicted in Fig. 3(c) show peaks for certain values of the de Haas-van Alphen frequency F. Since the Fermi surface of Bi consists of three electron ellipsoids and one hole ellipsoid [see Fig. 1(b)], there should be at the most four frequencies and their harmonics. For **B** exactly along the trigonal axis the three electron frequencies are degenerated ($F_e = 8.72$ T and $F_h = 6.34$ T [9]). The range of possible frequencies of electrons for a deviation of **B** of up to 5° with respect to the trigonal axis (this is our worst case estimate) are sketched in the Fourier plots as a shaded bar. For the holes, F_h is the minimum value and the variations for a tilt within 5° are small [9]. The Fourier amplitude of the sweep in Pos H shows an intense peak near F_h and additional peaks at the first and second harmonics. At Pos E the peak at F_h is reduced but another peak develops at $F = 10.3$ T that could be interpreted as one of the electron peaks for a small tilt between the field and the trigonal axis. Since all the high field sweeps are recorded with the same field orientation, the frequencies of the Fourier peaks should be the same. However, we observed the nonexpected result that the amplitudes of the peaks depend on the position of the excitation with respect to the collector PC.

In conclusion, the strong influence of a longitudinal magnetic field on the carrier propagation emerging from a pointlike source has been demonstrated by using a real space resolving scanning technique. Proceeding from the established situation at zero magnetic field, several new effects have been shown for the first time by light-induced carrier excitation. Longitudinal electron focusing was observed by reproducing the Sharvin experiment with light-induced carrier excitation instead of carrier injection through a point contact.

At low magnetic fields we observed Sondheimer oscillations. With our real space scanning technique it is possible to identify the contributions of electrons and holes due to the evolution of their focusing patterns in a longitudinal magnetic field. Additional contributions that are probably related to the anisotropic magnetoresistance were observed at magnetic fields of several 10 mT. At high magnetic fields we observed light induced magneto-oscillations due to Landau quantization with an amplitude depending on the position of excitation. The further development of this technique could lead to deeper insights into the physics of magneto-oscillations by the possibility of their systematic spatially resolved observation. Moreover, in the context of the earlier results already obtained using this innovative technique, the new observations presented in this Letter underline the potential of the method and its evolution in the future.

[1] W. Ashcroft and D. Mermin, Solid States Physics (Saunders College Publishing, Forth Worth, 1976).
[2] Yu. V. Sharvin *et al.*, Zh. Eksp. Teor. Fiz. Pis'ma Red. **1**, 54 (1965) [JETP Lett. **1**, 152 (1965)].
[3] J. Heil, M. Primke, K. U. Würz, and P. Wyder, Phys. Rev. Lett. **74**, 146 (1995).
[4] M. Primke, J. Heil, and P. Wyder, Physica (Amsterdam) **218B**, 26 (1996).
[5] J. Heil *et al.*, Phys. Rev. B **54**, 2280 (1996).
[6] J. Heil, A. Böhm, M. Primke, and P. Wyder, Rev. Sci. Instrum. **67**, 307 (1996).
[7] V. S. Edelman, Adv. Phys. **25**, 555 (1976).
[8] D. Weiner, Phys. Rev. **125**, 1226 (1962).
[9] D. Shoenberg, Magnetic Oscillations in Metals (Cambridge University Press, Cambridge, 1984).
[10] I. F. Sveklo and V. S. Tsoi, Zh. Eksp. Teor. Fiz. **103**, 1705 (1993).